The 2012 World Congress on
Advances in Civil, Environmental, and Materials Research (ACEM' 12)
Seoul, Korea, August 26-30, 2012

Structural Behavior Analysis of UHPCC Hybrid Tower for MW Super high Wind Turbine under Rated Wind Load

*Xiang-Guo Wu[1)], Jing Yang[2)], Si-Yuan Chen[3)], Qun Yu[4)] and Sang-Mook Han[5)]

[1)] *School of Civil Engineering, HIT, Harbin 150001, China*
[1)] *wuxiangguo@hit.edu.cn*
[2-4)] *School of Architecture Engineering, HEU, Harbin 150001, China*
[5)] *School of Civil Engineering, KIT, Gumi 730-701, Korea*

ABSTRACT

Based on the design conception of advanced wind turbine tower system, Ultra High Performance Cementitious Composites with compressive strength 200MPa(UHPCC-200) is proposed for the structural design of super high hybrid wind turbine tower over one hundred meters height to gain durable, ductile and high strength design objectives. The structural design proposal is introduced firstly including the design parameters for 3MW wind turbine. The material properties, mixing compositions and simplified constitutive relation and model parameters are outlined in the second section. Using nonlinear finite element analysis, the effects of wall thickness, wall thickness ratio and prestressing tendon on the structural longitudinal stress field, lateral displacement, stress mutation at transition zone between the middle segment and the bottom segment are calculated and analyzed. Based on the stress field analysis, the design limitation of the segmental wall thickness and its ratio are recommended. Checking formula of the longitudinal stress and lateral displacement are proposed by regression analysis of the numerical results finally. This paper will be a reference for the super high UHPCC hybrid tower for engineering design.

1. INTRODUCTION

As the support component of a wind turbine system, wind turbine tower is used to lift the sails at design height ensuring the wind turbine to gain stable wind resources. Enough strength, stiffness and stability are required for the support component (Arthouros 2008; Zhang 2009). Recent years, ultrahigh wind turbine tower i.e. over one hundred meters height is one important developing direction for MW degree wind turbine system to gain more stable wind speed. However, the section diameter of the

[1)] Associate Professor
[2-4)] Graduate Student
[5)] Professor

super high steel tower will greater than the nowadays highway transportation limit of 4.2m. Moreover, steel tower's cost is high and its durability is low. To solve the highway transportation difficulty, develop durable and ductile tower, developing hybrid tower with cementitious material taper cylinder part and short steel taper cylinder part is one ideal selection. Based on the conception of Advanced Wind Turbine System (ATS) (The Concrete Centre 2007; Eize 2009; Brughis 2004), Ultra High Performance Cementitious Composites (UHPCC) is proposed for the super high wind turbine tower design here. A new generation of light weight high performance wind turbine tower with durable, ductile behaviors is formed using prefabrated UHPCC segment assemble technology and external prestressing technologies.

UHPCC is obtained by mixing short and thin steel fiber, a high strength cementitious matrix, and mineral admixtures with a special mixing technique and curing system. UHPCC exhibits high mechanical and durability properties with compressive strength in the range 80-400MPa, tensile strength 10-30MPa, and elastic modulus 40-50GPa. UHPCC is an advanced material with many superior performance factors and is a new generation of engineering structural material that will replace normal strength concrete and normal high strength concrete in future designs (Wu and Xu 2009). Recently, a number of researchers have carried out extensive researches and engaged in international communication in the areas of material strain hardening behavior (Wu and Han 2009; Wu, Han and Xu 2008), constitutive property behavior of UHPCC (Williams et al 2010), strength model (Ramadoss and Nagamani 2008), UHPCC behavior under multi-axial compression (Kittinun et al 2010), and interface performance of UHPCC hybrid elements (Wu and Han 2010). Some new types of structures employing UHPCC were applied such as Shepherds Creek Bridge in Australia (Cavill et al 2003), Wapello Bridge in Iowa, USA (Graybeal et al 2004), Kuyshu High Speed Bridge in Japan (Okuma 2004), FHWA short span bridge in the USA (Graybeal et al 2004), the Saint-Pierre-La-Cour hybrid bridge in France (Behloul 2007), and UHPCC permanent form in China(Wu, Zhao and Han 2012). However, super high wind tower design with prefabricated UHPCC segmental element is a new and challenging area since the complixities of the loads environments.

In super high UHPCC hybrid tower design, different segmental wall thickness compositions effect the structural general design proposal. Therefore, segmental wall thickness and wall thickness ratio between middle part and bottom part are important parameters for the structural design. In addition, prestressing force should be also considered since it also effects on the structural deformation. Based on the description of general design proposal of the ultrahigh hybrid tower, the effects of segmental wall thickness, wall thickness ratio and prestressing force on structural performance under rated load model are analyzed using nonlinear finite element. This paper will be a reference for the new type of super high, durable and ductile wind turbine hybrid tower design for engineers.

2. PROPERTIES OF UHPCC

UHPCC with compressive strength 200MPa is proposed for the high performance hybrid tower design and the material is noted as UHPCC-200 in this paper. Properties of UHPCC-200 including mixing compositions, mechanics and durability properties are

introduced here briefly. More precise information and its constitutive model can be referenced from properties introductions of UHPCC (Wu, Zhao and Han 2012).

2.1 Mixing compositions of UHPCC-200

Mix compositions of UHPCC-200 are shown in Table 1. Fine silica sand is substituted by normal sand from the Songhua River to reduce the material cost. The steel fiber mixing volume fraction is 2% of the composites. Precise information of the composites material and mixing technique of UHPCC can be obtained from (Wu, Zhao and Han 2012).

Table 1 Mixing compositions of UHPCC-200 (kg/m3)

Cement	Silica fume	Filling powder	Fine sand	Super Plast.	Water	Expan. agent	Defoamer	Steel fiber
798.45	213.43	161.56	864.74	33.48	164.71	3.95	3.95	108.36

2.2 Mechanics behavior of UHPCC

According to the results of the uniaxial tensile test and cylinder splitting test, the tensile strength of the UHPCC-200 is about 15MPa to 25MPa, which is dependent on fiber parameters such as steel fiber volume fraction. This tensile strength is about 6 to 8 times that of normal strength concrete (NSC). Therefore, The tensile stress zone cannot be omitted in the UHPCC hybrid structure analysis which is the main difference from normal reinforced concrete structure.

For simplification and conservative analysis, the first tensile cracking strength of UHPCC-200 is selected as 6MPa. The strain hardening region is omitted here. The uniform elastic modulus is equal to 45GPa for UHPCC-200. This simplification agrees well with the model of UHPCC proposed by FHWA Report (Benjamin 2006) as shown in Fig. 1. Corresponding parameters value are listed in Table 2.

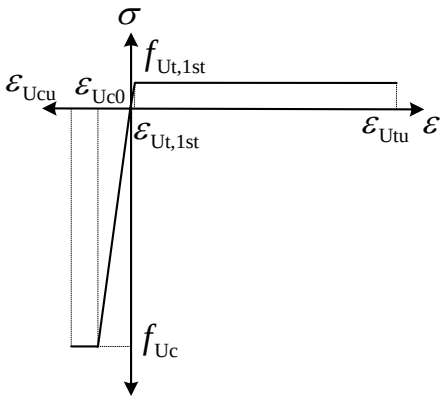

Fig. 1 Simplified stress-strain model of UHPCC

Table 2 Parameters of UHPCC simplified constitutive model

Para meter	The first tensile cracking strength	The first tensile cracking strain	Ultimate tensile strength	Ultimate tensile strain	Elastic Modul us	Poison ratio	Compress ive strength	Ultimate compressive strain

Value	6-8MPa	0.0001	15MPa	0.0025	45GPa	0.18	200	0.0036

2.3 Durability of UHPCC-200

The resistance ability of chloride attack of UHPCC-200 is about two Coulombs based on ASTM 1202 which is rather higher than NSC and FRC (Fiber Reinforced Concrete). The resistance of freezing-thawing is also very high with almost 100 percent of relative dynamic elastic modulus remaining after 600 cycles according to ASTM C 666B. Table 3 shows the comparisons of UHPCC-200 durability items with NSC and HSC/HPC (high strength concrete/high performance concrete).

Table 3 Durability Comparison of UHPCC with NSC and HSC/HPC

Property		NSC	HSC/HPC	UHPCC-200	Measurement
Resistance of Chloride attack (Coulombs)		2,445	178	1.5	ASTM C 1202
Neutralization (depth: mm, 6 month)		17	3.5	0	CO_2 10%, RH 60%, 30℃
Resistance of Freezing-Thawing (Relative Dynamic Elastic Modulus: %, 600 cycles)		78	95	100	ASTM C 666 B
Permeability	Air permeability (X10-16m2)	0.1335	0.0475	0.01	Direct Pressure
	Water Permeability (mm2/sec·Bar)	0.00362	0.00259	0.000374	
	Permeability (Coulombs)	776	135	0.9	ASTM C 1202
Porosity (ml/g)		0.1605	0.0874	0.0452	Auto Pore 9220

3 DESIGN PROPOSAL OF UHPCC HYBRID TOWER

The design objective of this high performance hybrid tower is to support 3MW wind turbine system which main technical parameters are shown in Table 4(Staffan, Tomas and Manouchehr 2010). The design height is 120m and the tower is divided into three parts[16], i.e. upper steel cylinder part, middle UHPCC taper cylinder part and bottom UHPCC taper cylinder part as shown in Fig. 2. The height of the upper steel is 2m and its wall thickness is 20mm. The middle and bottom parts are constructed by prefabricated UHPCC segment. The total height of these two parts is 118m. The middle part which assembles height is 98m is connected with the upper steel cylinder part. The design variable of the middle part wall thickness is selected from 100mm to 200mm. The design height of the bottom taper cylinder is 20m and its design variable of wall thickness is selected from 150mm to 300mm. The parts interfaces are connected by interval flexible bolt and external prestressing tendon as shown in Fig. 3. To satisfy highway transportation requirement, the middle and bottom UHPCC parts are separated into several UHPCC longitudinal prefabricate segment. There are totally 23 segments with design height 5m in which four segments are in the bottom part and

nineteen segments are in the middle part. There is another segment with design height 3m on the top of the middle part. The adjacent segments are connected with interval flexible bolts. The three parts are perforated overall using external prestressing tendon from the top to the tower base. The top and bottom of each UHPCC segment element are arranged with one ring rib which is used for the anchorage of prestressing tendon and bolt connection. The design diameter of the tower base and the top of the tower are 12m and 3m, respectively. Every hole is arranged with six prestressing tendon. Eight holes on every ring rib are arranged with prestressing tendons and total 48 tendons are used here. Other four holes are arranged with bolt connection.

Table 4 Main parameter of wind turbine

Rated Power	3MW	number of blade	3 个
The wheel hub in the rated wind of height V	13.5 *m* / *s*	cut-in wind speed	3.5 *m* / *s*
power control mode	variable speed adjustable pitch	cut-out speed	25 *m* / *s*
Unit safe level	IEC IB	rotor speed	9-17rpm
hub height	123m	Sweep area	7850 m^2
rotor diameter R	100m	mainshaft tilt angle	7°
Impeller weight G_1	85t	Cabin weight G_2	127t

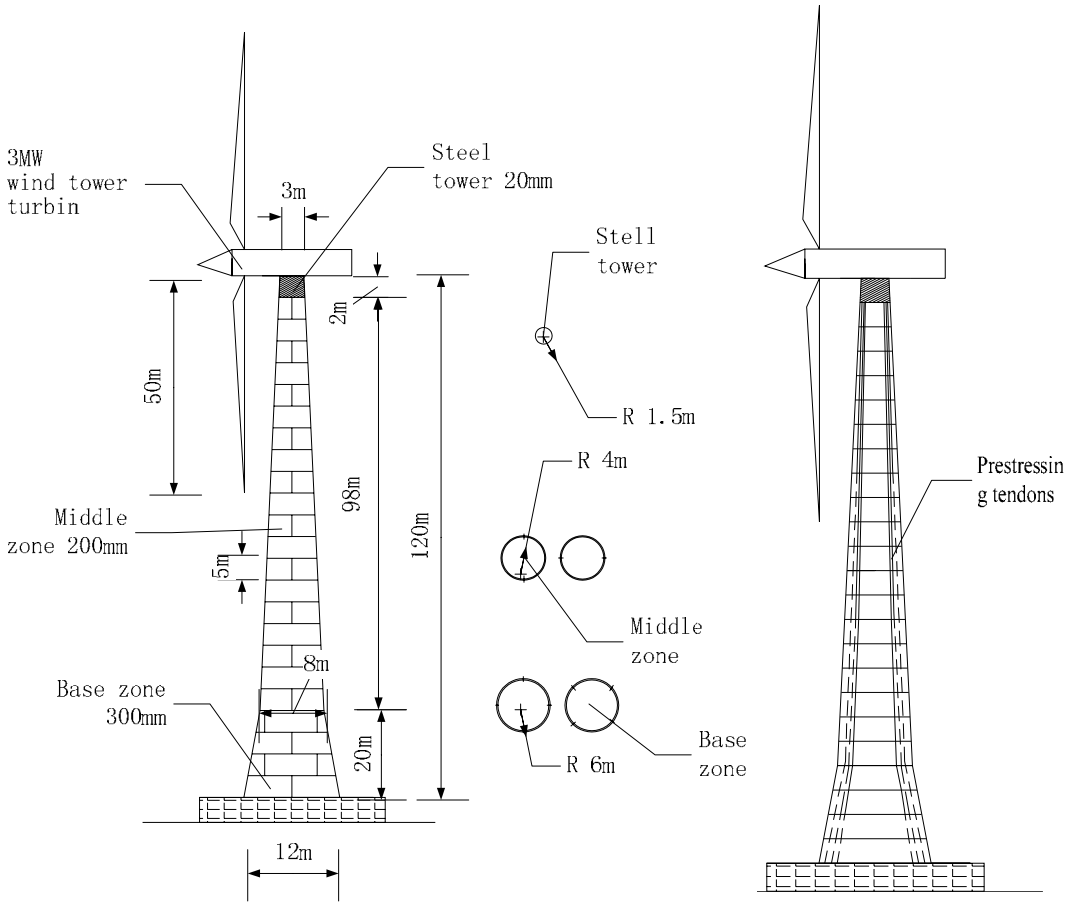

(a) Three parts and segment (b) Prestressing tendon

Fig.2 Main part of the tower

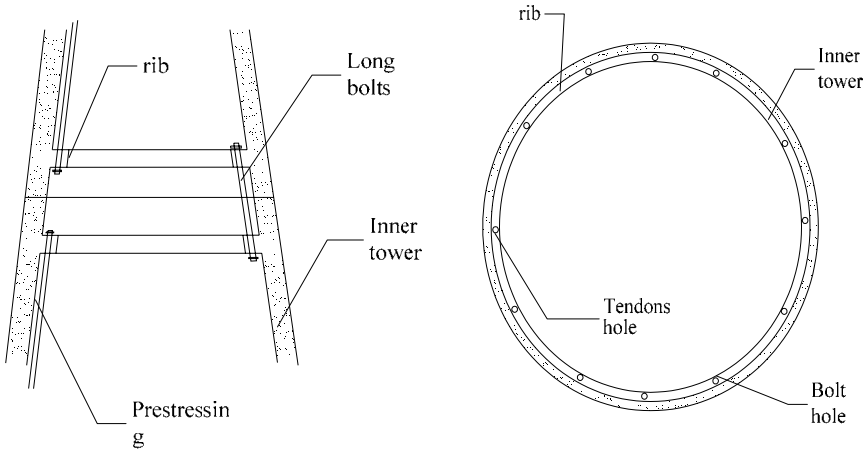

(a) Bolt connection (b) Segment cross section

Fig.3 Local detailed diagram

4. LOAD MODEL AND PARAMETERS

For MW wind turbine system, the loads carried by the tower includes the tower self-weight, turbine weight, top moment due to the eccentricities of wind wheel and engine room from the tower axies, horizontal thrust on wind wheel and longitudinal distributed load of wind load.(Li 2004)(Chen 2010)

4.1 Top concentrated load

According to the force analysis, the structure can be simplified as a variable cross-sectional cantilever beam with longitudinal distributed wind load, top concentrated load such as the selfweight of engine room, hub, lamina and the top concentrated moment due to the concentrated load eccentricity (Zhao and Lv 2009)(Bai H.Y.2010). The tower coordinate original point is defined as the intersection point of tower axis and tower top upper surface (Gu 2009) as shown in Fig. 4(a) in which X is the direction along the axis of wind wheel and fixed with tower, Z is the normal direction of the upper surface, and Y is the direction determined by right hand rule.

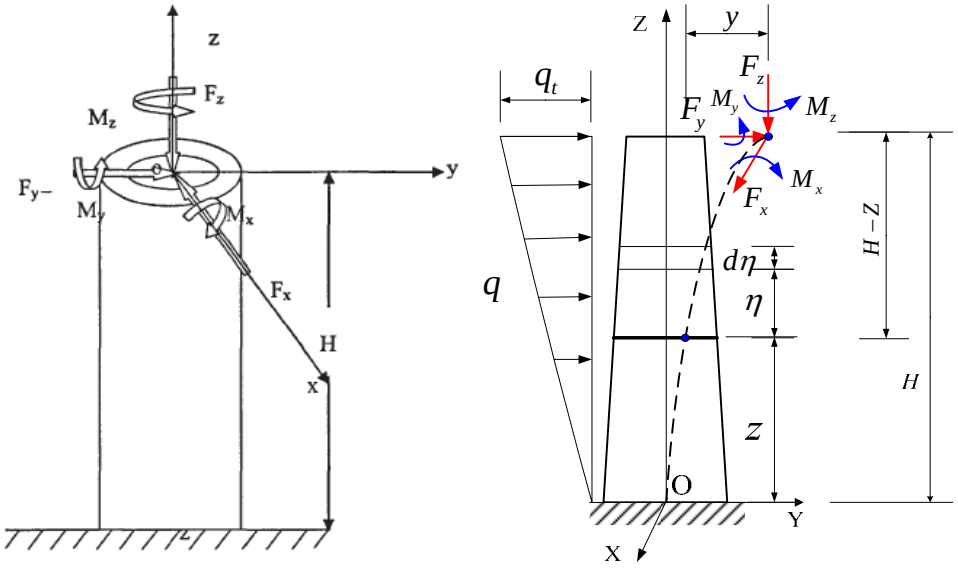

(a) Top concentrated loads (b) Mechanic model

Fig.4 The coordinate system of tower top upper surface

Here, F_x is aerodynamic thrust on wind wheel, F_y is pulsating force on laminas, F_z is the tower axial compressive force, M_x is the pitching moment due to wind wheel and engine, M_y is the pitching moment resulted from gradient, M_z is the torsion from wind wheel. The calculation formula of F_x, F_y, F_z, M_x, M_y and M_z are listed in Table 5.

Table 5 Calculation formula of the top concentrated loads

No.	Load	Calculation formula
1	F_x	$F_x = \frac{4}{9}\rho\pi R^2 V^2$
2	F_y	$F_y = \frac{1}{9}\times\frac{\rho}{3}\pi R^2\left(V_1 - V_2\right)^2$
3	F_z	$F_z = G_1 + G_2$
4	M_x	$M_x = \left(G_2 - G_1\right)\times h$
5	M_y	$M_y = \frac{8}{27}\frac{\rho}{3}\pi R^3\left(V_1^2 - V_2^2\right)$
6	M_z	$M_z = \frac{1}{2}\rho U_\infty^2\pi R^3\lambda\left\{\int_0^R \mu^2\left[8a'\left(1-a\right)\mu - \frac{W}{U_\infty}\frac{N\frac{c}{R}}{\pi}C_d\left(1+a'\right)\right]d\mu\right\}$

In which, ρ is air density (kg/m^3), R is diameter of wind wheel (m) and V is the rated wind speed at the rub-height of wind turbine (m/s). With V_1 and V_2 are the wind speed

on the top and bottom of wind wheel, respectively (m/s). Wind speed *V* at height of H can be written as (MHURD of PPC 2002)(Jiang 2009).

$$\frac{V}{V_0}=\left(\frac{H}{H_0}\right)^{\alpha} \tag{1}$$

In which, V_0 is wind speed value at height of H_0 which is usually selected as 10m from ground (m/s). α is the wind shear coefficient and its span is between 0.1 and 0.4. G_1 is wind wheel gravity and G_2 is engine gravity. *h* is the eccentricity distance. By substituting the parameters in Table 4 to the calculation formula, the tower top load can be calculated as shown in Table 6.

Table 6 Loads on the top of the tower

Load condition	$F_x(KN)$	$F_y(KN)$	$F_z(KN)$	$M_x(KNm)$	$M_y(KNm)$	$M_z(KNm)$
Rated load	763. 02	8.4	2077.6	4116	2376.5	282.29
Ultimate load	1261.67	27.81	2077.6	4116	3456.7	969.993
Storm load	1883.25	37.54	2077.6	4116	4704.09	1309.5

4.2 Wind load model

The standard value of the wind load on unit area of high rise structure can be expressed as

$$w_k=\beta_z\mu_s\mu_z\omega_o \tag{2}$$

In which, β_z is the gust response coefficient and equals 1.43 for this hybrid tower. μ_s is shape factor of wind load and equals 0.57 according to the structural load code (MHURD of PPC 2002). μ_z is the high wind pressure coefficient of variation and equals 2.5 for this hybrid tower. ω_o is the fundamental wind pressure and $w_o=0.5\rho v^2$ =109.35 N/m^2 . The standard value of wind load can be calculated and equals to 222.83 N/m^2 for the hybrid tower under rated wind load.

4.3 Longitudinal stress field

The tower can be simplified as a taper cylindrical cantilever beam with reduce section. The self weight of the turbine engine, hub and laminas are modeled as the concentrated loads in the top of the tower. The moments of the concentrated loads due to the eccentricities are considered simultaneously. The origin point of the coordinate system is selected at the center of the base section. The mechanic model is shown in Fig. 4(b). Under the loads action, the total moment on the section with distance z from the base section can be theoretically expressed as(Song Xi 2011)

$$M = F_y\left(H - z + h_1\right) + F_z y + M_x + M_y + M_z + \frac{1}{H}\int_z^H q_t\left(z + \eta\right)\eta d\eta \quad (3)$$

In which, H is the tower height, y is the second order eccentricity due to the structural deformation and h_1 is the distance of wind wheel center from the top of the tower. Due to the second order eccentricity is small, $F_z y$ can be omitted in practical calculation. According to elasticity theory, the sectional normal stress can be written as

$$\sigma = \frac{M}{\frac{\pi D^3}{32}\left(1-\alpha\right)^4} = \frac{F_y\left(H - z + h_1\right) + q_t\left(2H^3 + 3H^2 z - z^3\right)/\left(6H\right) + M_x + M_y + M_z}{\frac{\pi D^3}{32}\left(1-\alpha\right)^4} \quad (4)$$

Here, *d* and *D* are inside and outside diameters of the section, respectively.

5 FINITE ELEMENT ANALYSIS OF THE HYBRID TOWER

Based on the design proposal of the UHPCC hybrid tower, numerical analysis using ABAQUS is carried out here by different wall thickness composition. Firstly, three wall thickness compositions with fixed wall thickness ratio 2:3, i.e. 200-300, 140-210, 100-150, are used to study the effect of wall thickness on UHPCC tower stress field and deformation development. Secondly, three wall thickness ratio compositions i.e. 3:6, 4:6 and 5:6 are used to study the effects of wall thickness ratio on UHPCC tower stress field distribution and deformation development and the corresponding wall thickness compositions are 100-200, 200-300, and 200-240, respectively. Material density of UHPCC-200 is 2500 Kg/m^3, material modulus of 4.5e10Pa and Poison ratio is 0.2. Smear crack model is used here to analyze the structural general responses. Tensile plastic strain is equal to 0.0016.

Prestressing tendons 1×7 are used here for one prestressing bar with diameter 15.2mm and ultimate tensile strength 1860MPa, density 7850 Kg/m^3, coefficient of linear expansion 1.263e-005, elastic modulus 1.95e11MPa, Poison ratio 0.3 and prestressing stress 1231MPa.

The tower is divided into seven parts in which part1 to part4 are the segments of the bottom part from the base to middle part, part5 is one segment of middle part. Prestressing bar is numbered as part6 and part7. Three dimensional solid elements C3D4 is used to the UHPCC part1 to part5. Truss element is used to the prestressing bar element part6 and part7. The failure ratio and tension rigidization input values are shown in Table 7 and Table 8, respectively.

Table 7 Failure rate of UHPCC-200

Ratio 1	Ratio 2	Ratio 3	Ratio 4
1.18	0.06	1.25	0.033

Table 8 Tension rigidization of UHPCC-200

	1	2	3
Sigma/sigma_c	1	1	0
Eplison-eplison_c	0	0.0096	0.0098

Two analysis steps are used here (Kai, Huang, Huang 2006). Firstly, predefined filed type temperature method is used to tension prestressing bar. And then, load is

applied to the model. In the module of interaction, tie bind is applied between the segments. In the load step, all the displacements on the base are fixed firstly. And then, gravities, longitudinal distributed wind load and tower top load including three directions of the concentrated loads and concentrated moments are applied. Due to large dimension of the tower, methods of structured and sweep edges are all used during mesh (Gu 2009)(Li 2004). The mesh result is shown in Fig. 5.

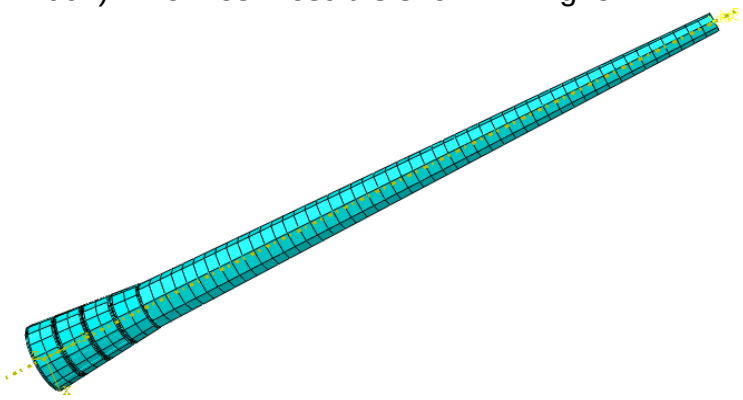

Fig.5 Mesh result of the UHPCC tower

6 STRENGTH ANALYSIS OF THE TOWER UNDER RATED WIND LOAD

6.1 Effects of wall thickness

Three wall thickness compositions, i.e. 200-300mm, 140-210mm and 100-150mm, are studied here with fixed wall thickness ratio 2:3. The distributions of longitudinal stress of the tower on windward side and leeward side are shown in Fig. 6 (a) and (b).

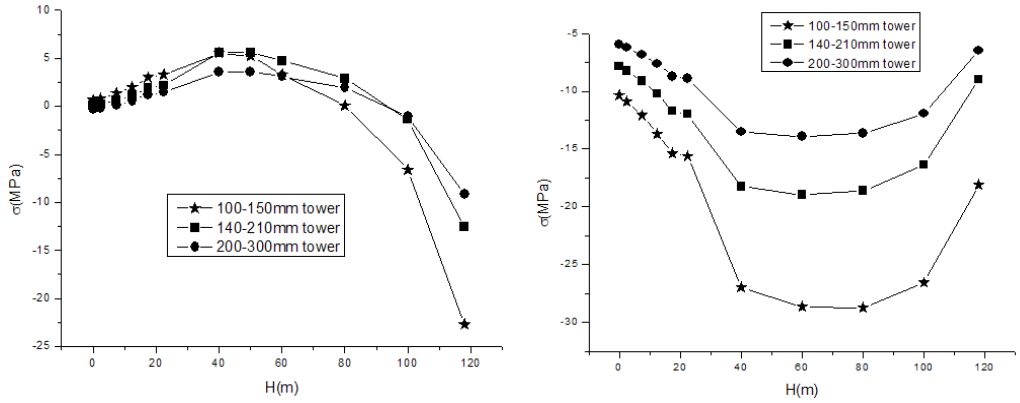

(a) Windward side (b) Leeward side

Fig.6 Longitudinal stress distribution of UHPCC segment

As shown in Fig.6 (a), stress distributions of 140-210 and 200-300 wall thickness compositions are close with similar trend, whereas the stress distribution of 100-150 wall thickness composition deviates from the general trend of 140-210 and 200-300 wall thickness composition. The stress on windward side of UHPCC segment 40 meters from the base is tensile and increases linearly with the height increasing. From

the stress formula of cantilever reducing sectional bending beam, variations of moment and sectional inertia moment result in the stress and sectional curvature variations. Therefore, the curvature increases linearly in the first 40 meters of the bottom part. Under prestressing force action, sectional tensile stress decreases. With the height increasing in the region over 40 meters, sectional tensile stress decreases, i.e. sectional curvature decreases until naught stress in the 80-100 meters zone for 200-300 and 140-210 wall thickness composition hybrid tower. And then stress on windward side turns into compression. For 100-150mm composition tower, the tension and compression boundary is around 60 meter zone.

As shown in Fig. 6(b), the leeward side is all in compression. In the first 40 meters zone, compressive stress increases linearly with the height and this can also be explained using variation of the curvature along the tower. From 40 meters to 100 meters, stress variation is relative smooth. For 200-300mm and 140-210mm wall thickness composition, compressive stress reaches at the maximum and less than 30MPa. Whereas the maximum compressive stress is around 80m position for 100-150mm wall thickness composition. In the region beyond 100m, compressive stress decreases with increasing of height which is resultd by the decreasing of the curvature.

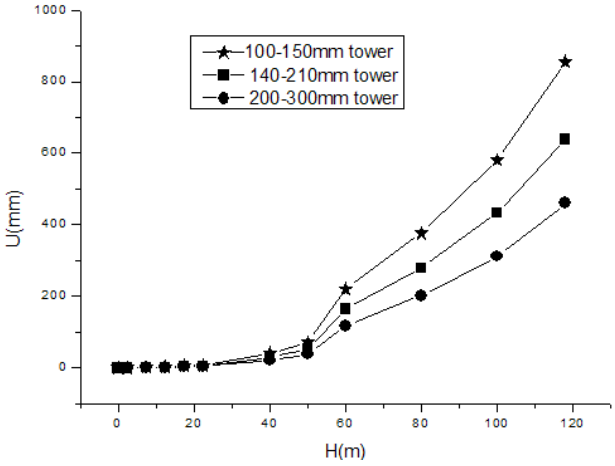

Fig.7 Displacement distribution with height

As shown in Fig. 7, the maximum displacement is on the top of the tower. The longitudinal deformation belongs to flexural type. In the first 50 meters zone, the displacement variation is small and then the joint displacement increases obviously. Normally, the allowable deformation of the tower top is about 0.5-0.8% of the tower height. According to the calculation results, the maximum lateral displacement of the tower top is 0.113% of the height. In addition, the joint displacement at 80m coordinates are 201.46mm, 279.91mm, 376.02mm for the three wall thickness compositions towers, respectively. The displacement differences of the three wall thickness tower at 80m coordinates are 78.48mm and 96.11mm. The joint displacement at 60m coordinates are 117.57mm, 163.76mm, 219.95mm for the three wall thickness compositions towers, respectively. The displacement differences of the three wall thickness tower at 60m coordinates are 46.20mm and 56.18mm. The joint displacement at 100m coordinates are 311.81mm, 432.16mm, 580.11mm for the

three wall thickness compositions towers, respectively. The displacement differences of the three wall thickness tower at 100m coordinates are 120.35mm and 147.95mm. Corresponding displacement incremental ratios are 1.216, 1.224 and 1.229 which implies that the displacement incremental distribution is linear in the zone over 60 meters.

The non-dimensional tensile stresses and the lateral displacements on the windward side of the tower are shown in Fig. 8(a) and (b) with the variations of wall thickness. The variations curves of the tensile stress and lateral displacements with the wall thickness are regressed and corresponding simplified checking formula are proposed as shown in equations (5) and (6).

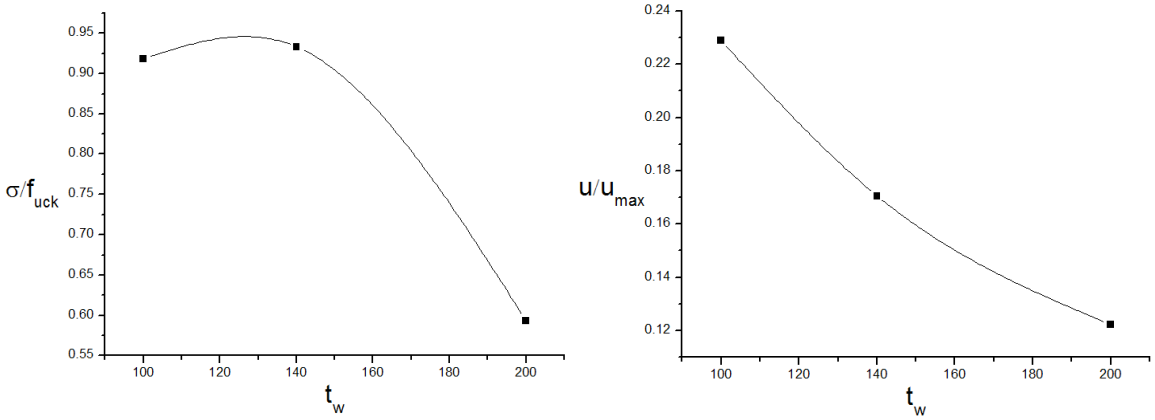

(a) Non-dimensional tensile stress (b) Non-dimensional lateral displacement

Fig.8 Regression curves with wall thickness

$$\frac{\sigma}{f_{uck}} = 0.04 + 0.015t_w - 0.00006{t_w}^2 \quad (5)$$

$$\frac{u}{u_{\max}} = 0.47 - 0.003t_w + 6.06e(-6){t_w}^2 \quad (6)$$

In which, f_{uck} is the initial cracking strength of UHPCC-200 (MPa), t_w is the wall thickness (mm), and $u_{\max}$ is the maximal allowable lateral displacement (mm).

6.2 Effect of wall thickness ratio

Calculation results of stress and deformation of the tower with three wall thickness ratio compositions 3:6, 4:6 and 5:6 are shown in Fig.9(a) and (b). The corresponding wall thickness compositions are 100-200mm, 200-300mm and 200-240mm, respectively.

As shown in Fig. 9(a), tensile stress increases with the height coordinates linearly in the first 40 meters zone. In the zone of 40-80 meters, stress variation on wind ward is smooth for 200-300mm and 200-240mm compositions tower. Over 80 meter height, stress on windward side turns into compression state. For 100-200mm composition tower, the maximum tensile stress is greater than 5MPa and the neutral point is around 60m coordinate, i.e. stress turns into compression over 60m coordinates.

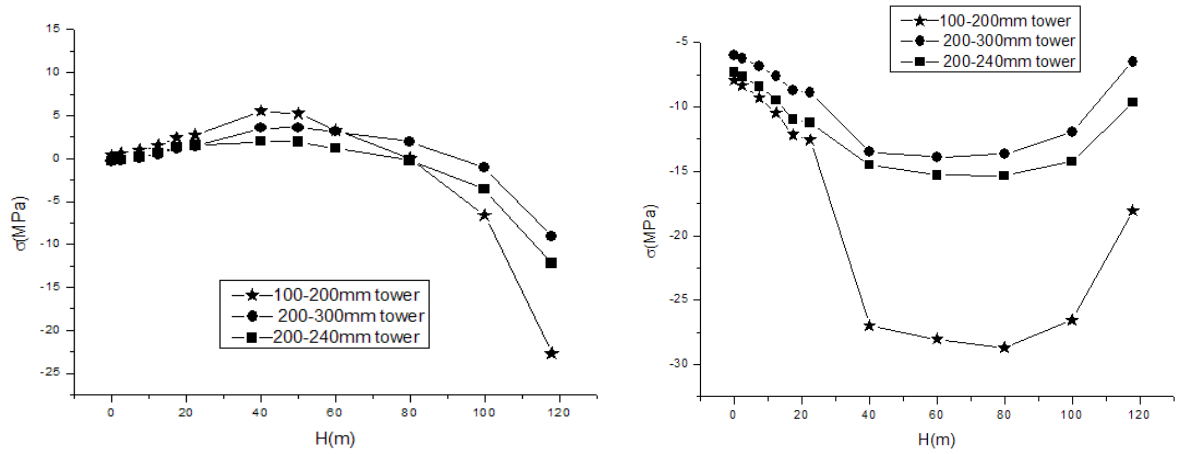

(a) windward side (b) Leeward side

Fig.9 Stress distributions with three wall thickness ratio compositions

As shown in Fig. 9(b), the tower leeward side are all in compression. In the first 40 meters zone, stress increases with the height. In the zone between 40m and 100m, the variation of the stress is small. Maximum compressive stress locates at 60m coordinates and less than 30MPa. Stress variation of the tower with wall thickness ratio 4:6 and 5:6 is smooth, whereas the variation of the tower with wall thickness ratio 1:2 is large which indicates that stress variation is steeper with wall thickness ratio decreasing. It also can be seen from Fig. 8(b) that the stress increment variation is nonlinear with wall thickness ratio variation. The stresses at 60m coordinate are -13.91MPa, -15.48MPa and -27.64MPa for wall thickness ratio compositions 3:6, 4:6 and 5:6, respectively and the differences are 1.57MPa and 12.16MPa. The stresses at 80m coordinate are -13.62MPa, -15.62MPa and -28.97MPa, respectively. The differences are 2.0MPa and 13.35MPa.The stresses at 100m coordinates are -11.95MPa, -14.25MPa and -26.56MPa, respectively and the relative differences are 2.30MPa and 12.31MPa. The differences ratios at the three coordinates are 7.736, 6.677 and 5.358 which indicates that the stress increments are nonlinear variation.

It can be seen from Fig. 10 that the lateral displacements in the first 50 meters zone are small. In the zone over 50 meters coordinate, the displacements increase with the height. The maximum displacement is 800mm for wall thickness 100-200 compositions which is in the allowable deformation limit 0.5-0.8% of the total height. The deformations of 200-300 and 200-240 are close and are approximate linear variation, whereas the deformation of 100-200 is big and is nonlinear variation. The displacements at 60m coordinates are 117.11mm, 117.55mm and 207.15mm for wall thickness ratio compositions 3:6, 4:6 and 5:6, respectively. The differences are 0.43mm and 89.60mm. The displacements at 80m coordinates are 198.65mm, 201.46mm and 359.34mm, respectively and the differences are 2.80mm and 157.89mm. The displacements at 100m coordinates are 305.72mm, 311.81mm and 559.66mm, respectively and the relative differences are 6.09mm and 247.85mm. The differences ratios at the three coordinates are 206.46, 56.35 and 40.70 which indicates that the displacement increments are nonlinear variation.

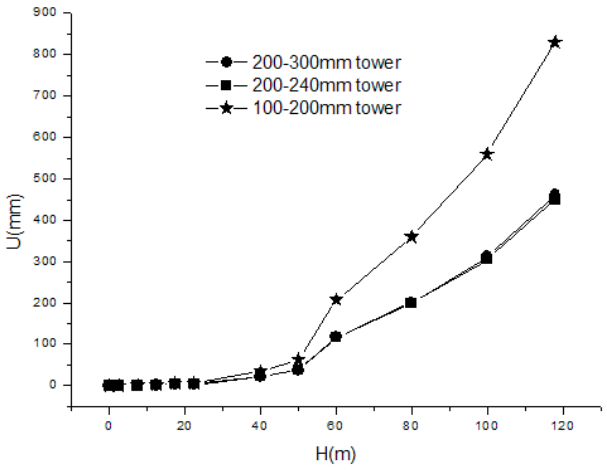

Fig.10 Displacement variation with three wall thickness ratio compositions

6.3 Effects of prestressing tendon on the structural general behaviors

To analyze the effect of prestressing force on structural behaviors of the hybrid tower, the longitudinal stress and lateral displacement distributions of the tower with 200-300mm wall thickness composition are calculated and compared between the tower with and without prestressing tendon layout as shown in Fig.11(a) and (b).

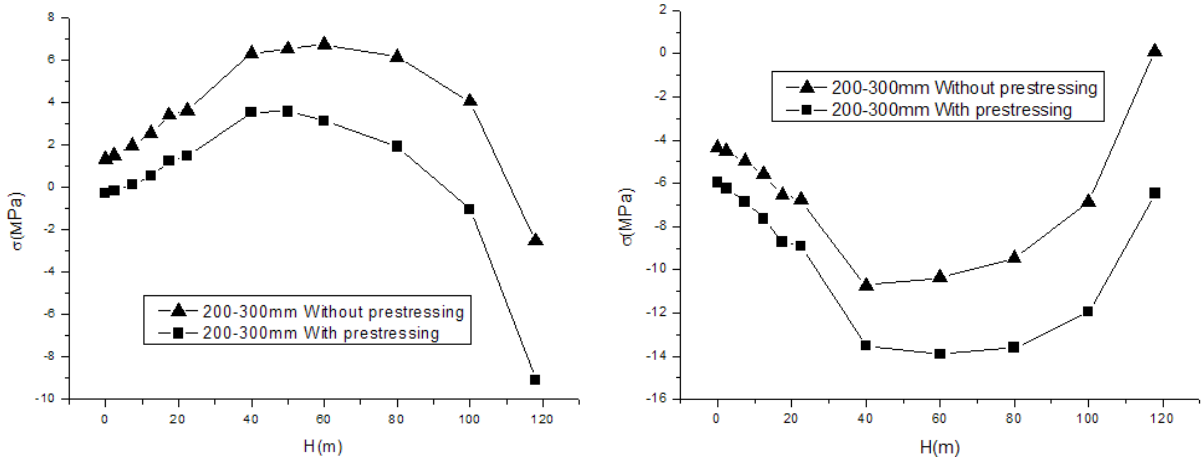

(a) windward side (b) Leeward side

Fig.11 longitudinal stress distributions

As shown from Fig. 11, the maximum tensile stress of the tower without prestressing action arrive at 7MPa under rated wind load which is greater than the material cracking strength. Under the prestressing tendon action, the tensile stress is reduced and the maximum stress is equal to 3MPa which is reduced about 50% compared with the tower without prestressing force. Hence, the prestrsssing tendon optimizes the tensile stress filed distribution effectively and improves the cracking strength of the hybrid tower.

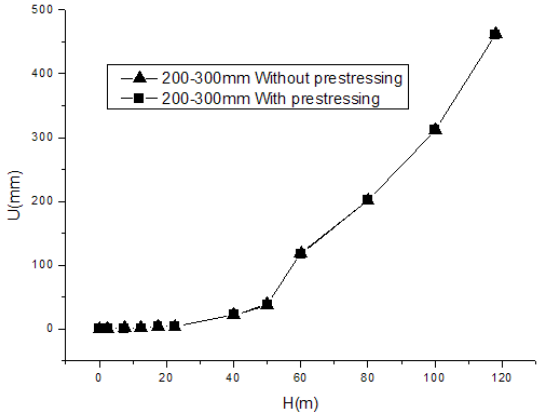

Fig. 12 Displacement distributions of the tower with and without prestressing

As shown in Fig. 12, the displacement increments of the tower with prestressing tendon are very small compared with the tower without prestressing action. This implies that the effect of prestressing action on the tower displacement tendon is very small.

The non-dimensional tensile stresses and the lateral displacements on the windward side of the tower are shown in Fig.13(a) and (b) with the variations of wall thickness ratio. The variations curves of the tensile stress and lateral displacements with the wall thickness ratio are regressed and corresponding simplified checking formula are proposed as shown in equations (7) and (8).

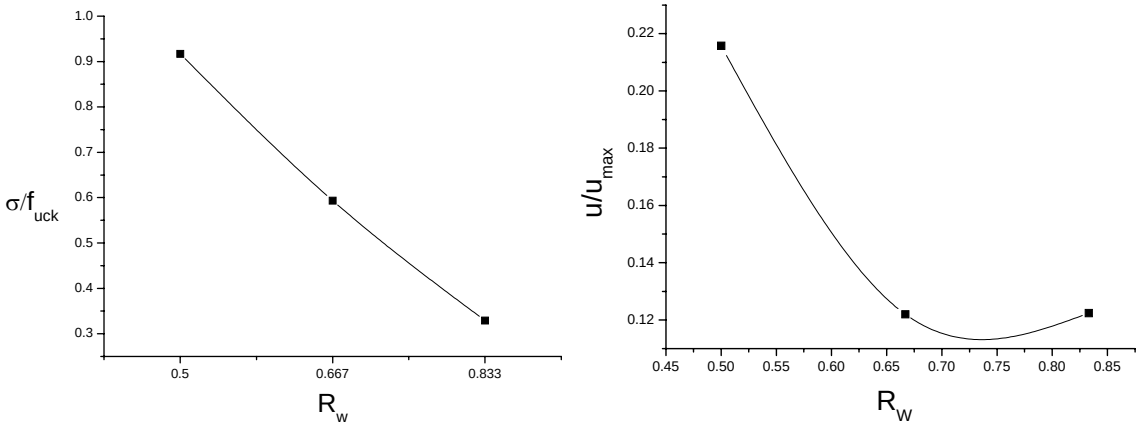

(a) Non-dimensional tensile stress (b) Non-dimensional lateral displacement

Fig.13 Regression curves of the tensile stress and lateral displacement

$$\frac{\sigma}{f_{uck}} = 2.23 - 3.14R_w + 1.03R_w^{\ 2} \tag{7}$$

$$\frac{u}{u_{\max}} = 1.06 - 2.54R_w + 1.69R_w^{\ 2} \tag{8}$$

In which, R_w is the wall thickness ratio.

7 CONCLUSIONS

The effects of wall thickness on structure stress distribution features and joint displacement: The peak value of the structural longitudinal stress distribution locates at the zone of 30m-60m. The peak values of these three typical wall thickness compositions approaches to the cracking strength of UHPCC-200. With the increasing of the middle part wall thickness, the peak value decreases and the general distribution of the longitudinal stress is smooth. The stress in leeward zone, joint compressive stress increases linearly with then increasing of wall thickness. Stress break exists in the transition zone between the middle part and bottom part. According the study, the minimum wall thickness for the middle part is proposed as 200mm. For ultra high tower, the full section are in compression at the longitudinal coordinates of 100m-200m. The effect of wall thickness on the bottm part displacement can be omitted according to the analysis. The middle part displacement increases linearly with the decreasing of middle part wall thickness.

The effects of wall thickness ratio on structural stress distribution features and joint displacement: With the increasing of wall thickness ratio value, the stress distributions with different wall thickness compositions are closed to each other and the stress in the parts transition zone is more continuous. With the wall thickness ratio decreasing, the stress distribution and displacement distribution are more nonlinear. wall thickness ratio has no effect on the joint displacement of the bottom part and the transition zone. The practical value of wall thickness ratio is proposed as 2/3 for engineering design.

Prestressing tendon effects on the structural response: The stress in the tension zone from 40m to 80m reaches the cracking strength of the material when there is no prestressing tendon. The stress is redistributed with the action of prestressing force. The stress level in the sensitive zone is controlled smaller than 3MPa, i.e. below the 50 percent of the cracking strength which indicates the cracking resistance strength of the structure is improved significantly. The section at the top of the middle part, i.e. 100-120m, is in full compression. Although the compressive zone stress increases about 30% compared with the tower without prestressing force, enough safety margin is ensures due to the UHPCC-200 with ultra high compressive strength is used here. In addition, effect of the prestressing force on the lateral displacement is very small. The effects of prestressing tendon can be omitted in the deformation control of the hybrid tower.

According to the calculation and analysis results of the super high tower only with several prestressing tendons, a little constructive reinforcement design in the peak stress zone, part transition zone is enough since the stress distribution and lateral deformation without reinforcement design are far away from the control state. The reinforcement design only based on the constructive requirements according to the reinforced concrete structure code.

ACKNOWLEDGEMENTS

The authors would like to thank the China National Natural Science Fund(51008088), the fundamental Research Funds for the Central Universities (Grant No. HIT. NSRIF.

2013112), the project sponsored by Harbin city science and technology innovation talents special funds(2011RFLXG014), and Heilongjiang Province Natural Science Fund (E200911) for providing funding to this project, and the Scientic Technical Plan of The Ministry of Housing and Urban-Rural Development of China(2010-K2-23) for the support to the authors work described herein.

REFERENCES

Bai H.Y. (2010), “The Finite Element Analyss Of Megawatt Level Generation Units Tower”, Taiyuan University of Technology, 2010 4, TM315 TM753.17-41.

Behloul, M. (2007), “HPFRCC field of applications: Ductal recent experience”, 5th High Performance Fiber Reinforced Cement Composite (HPFRCC5), Mainz, Germany, July.

Benjamin A. G. (2006), “Structural Behavior of Ultra-High Performance Concrete Prestressed I-Girders”. FHWA–HRT–06–115. August 2006.

Brughuis F.J.(2004), “Improved return on investment due to larger wind turbins”. Mecal Applied Mechanics BV P.O. Box 286, 7500AG, Enschede the Netherlands, www.mecal.nl.

Cavill, B. and Chirgwin, G.. (2003), “The worlds first Ductal road bridge Sherpherds gully creek bridge, NSW”, 21st Biennial Conference of the Concrete Institute of Australia, Brisbane.

Chen Y., Tian P., Liu X., Luo Z., Ye Z.Q., (2010), “Research on static and dynamic characteristics of cone-shaped tower of HAWTs”, Acta Energiae Solaris Sinica, 31(10): 1359-1365.

Eize de Vries. (2009), “Advanced Tower Systems (ATS) of the Netherlands inaugurated a prototype of itspatented concrete–tubular steel hybrid tower concept at one of Germany’s wind turbine test fields”, near Grevenbroich, Renewable Energy World September-october 2009.

Graybeal, B., Hartamann, J., and Perry, V. (2004), “Ultra-high performance concrete for highway bridge”, FIB Symposium, Avignon, 26-28 April.

Gu F.B. (2009), “The Research of Steel-Concrete Hybrid Tower of the wind Turbine”, Xinjiang Agricultural University, TM614 and TM642: 11-28.

Jiang F.J. (2009), “Large horizontal axis wind-driven generator cones form of finite element analysis and optimization tower design”, Inner Mongolia university of science and technology. TM315: 14-27.

Kai T., Huang A.X., Huang Q.H. (2006), “The finite element method and its application[M]”, Beijing：Science Press.

Kittinun S., Sherif E.T., and Gustavo P.M. (2010), “Behavior of high performance fiber reinforced cement composite under multi-axial compressive loading”, Cement & Concrete Composite, 32(2010): 62-72.

Li H.M. (2004), “Optimization Design and Analysis for Wind Turbine Tower Based on Finite Element Method”, Xinjiang Agricultural University, TU271.1: 13-27.

Ma L.H., Dai H.T., Zhang D.T., and Liu D.Y., (2008), “Design and Analysis for MW Wind Turbine Tower”, 2008 Annual Meeting of Clean & Effcient Coal Power Generation Technology Network, October 2008 Nanjing, China: 1-4.

MHURD of PRC(The Ministry of Housing and Urban-Rural Development of P.R.C.)(2002), *Load Code for The Design of Building Structures(GB50009-2001)*,China Architecture & Building Press, Beijing.(In Chinese)

Okuma, H., et al.(2006), “The first highway bridge applying ultra high strength fiber reinforced concrete in Japan”, 7th International Conference on short and medium span bridge. Montreal, Canada.

Ramadoss P. and Nagamani K. (2008), “A new strength model for the high-performance fiber reinforced concrete”, Computers and Concrete, 5(1): 21-36.

Song X. and DAI J.X. (2011), “Mechanical Modeling and ANSYS Simulation Analysis of Horizontally Axial Wind Turbine Tower”, Journal of Gansu Science, 23(1): 91-95.

Staffan, E., Tomas L., Manouchehr H., Thomas S. and John J.(2010), “Tall towers for large wind turbins”, .

Tricklebank A., Bromage A., (2007), “Concrete Towers for Onshore Wind Farms” The Concrete Centre, www.concretecentre.com: 16-26.

“Wind Turbine Generator system-Design Requirements”(The People's Republic of mechanical industry standard JB/T 100300-2001)

Wu X.G. and Han S.M. (2009), “Multiple cracking model of fiber reinforced high performance cementitious composite under uniaxial tension”, Int. J. of Concrete Structures and Materials, 3(1): 71-77.

Wu X.G. and S.M. Han S.M., (2010), “Interface shear connection analysis of Ultrahigh-Performance fiber-Reinforced concrete composite girders”, J. of Bridge Engineering(ASCE), 15(5), 493-50.

Wu X.G., Zhao X.Y. and Han S.M. (2012), “Structural analysis of circular UHPCC form hybrid pier under construction loads”. Steel and Composite Structures, An International Journal, 12(2): 167-181

Wu X.G., Xu S.L., Wu M.X. (2009), “Fracture parameters study and application of ultra high performance fiber reinforcement concrete”. **E**ngineering Mechanics, 26(3): 93-98.

Wu X.G., Han S.M., XU S.L. (2008), “Pseudo strain hardening model of ultra high performance cementitious composites under flexural loading”. Acta Materiae Compositae Sinica, 25(2): 129-134.

Williams E.M., Graham S.S., Akers S.A., Reed P.A. and Rushing T.S. (2010), “Constitutive property behavior of an ultra-high-performance concrete with and without steel fibers”, Computers and Concrete, 7(2): 191-202.

Zerous A. (2008), “Global development present situation and prospect of wind power”,China Energy, 30(4): 23-33.

Zhang W.L. (2009), “Research On Cone-shaped tower of MW grade wind turbine”, Shanxi University of Science and Technology, TM315: 15-22.

Zhao R.Z. and Lv G. (2009) , “Static Analysis of the Tower for Horizontal Wind Turhine Based on Finite Element”, Lanzhou University of Science & Technology, Compressor,Blower & Fan Technology ,2009（4）, TK83.

Zhao R.Z. and Lv G. (2009), “Based on the finite element method of the horizontal axis wind-driven generator, tower of the static analysis”, Lanzhou University of Science & Technology,2009, TM315.16-33.